CLIMATOLOGY

Extreme warmth and heat-stressed plankton in the tropics during the Paleocene-Eocene Thermal Maximum

Joost Frieling,[1]* Holger Gebhardt,[2] Matthew Huber,[3] Olabisi A. Adekeye,[4] Samuel O. Akande,[4] Gert-Jan Reichart,[5,6] Jack J. Middelburg,[5] Stefan Schouten,[5,6] Appy Sluijs[1]

Global ocean temperatures rapidly warmed by ~5°C during the Paleocene-Eocene Thermal Maximum (PETM; ~56 million years ago). Extratropical sea surface temperatures (SSTs) met or exceeded modern subtropical values. With these warm extratropical temperatures, climate models predict tropical SSTs >35°C—near upper physiological temperature limits for many organisms. However, few data are available to test these projected extreme tropical temperatures or their potential lethality. We identify the PETM in a shallow marine sedimentary section deposited in Nigeria. On the basis of planktonic foraminiferal Mg/Ca and oxygen isotope ratios and the molecular proxy TEX^{H}_{86}, latest Paleocene equatorial SSTs were ~33°C, and TEX^{H}_{86} indicates that SSTs rose to >36°C during the PETM. This confirms model predictions on the magnitude of polar amplification and refutes the tropical thermostat theory. We attribute a massive drop in dinoflagellate abundance and diversity at peak warmth to thermal stress, showing that the base of tropical food webs is vulnerable to rapid warming.

INTRODUCTION

Global ocean temperatures rapidly warmed by ~5°C during the Paleocene-Eocene Thermal Maximum (PETM) [~56 million years ago (Ma)] (*1*–*4*). This warming coincided with a global negative stable carbon isotope excursion (CIE) recorded in terrestrial and marine sedimentary components in conjunction with deep ocean carbonate dissolution, reflecting the injection of ^{13}C-depleted carbon into the ocean-atmosphere system (*1*). Reconstructions indicate that mid- and high-latitude temperatures met or exceeded modern tropical temperatures (24° to 29°C) during the PETM (*5*), which, based on climate model simulations, would require extremely warm (>35°C) tropics (*6*, *7*). These temperatures approach upper physiological limits for many extant organisms (*8*, *9*). Problematically, records in the subtropical-to-tropical latitude band (*10*–*12*) are often stratigraphically complex or incomplete, based on single proxies, or seem to be geochemically altered.

The lack of PETM proxy data from the tropics has hampered attempts to address questions essential for predicting future tropical climate change (*13*). For example, to what extent are tropical temperatures affected by greenhouse forcing, and what does this imply for tropical thermostat theory, meridional temperature gradients, and equilibrium climate sensitivity during the PETM? Furthermore, how was the biosphere affected in tropical near-shore environments (*14*)?

To assess these outstanding issues, we studied samples from boreholes IB10A and IB10B and the Sagamu Quarry (SQ) from the Oshosun Formation, Dahomey Basin, Nigeria (fig. S1). The Paleocene to Lower Eocene sediments of the Oshosun Formation were deposited on the shelf at 1°S to 7°S paleolatitude (*15*, *16*) and can be traced laterally over the Dahomey Basin (*17*). They typically consist of dark gray mudstones and are ~100 m thick in the IB10 cores. We generated organic and inorganic geochemical and micropaleontological data to locate the PETM and assess environmental change.

RESULTS AND DISCUSSION

We find planktonic foraminifer species indicative of Paleocene zones P4b, P4c, and P5 in the SQ and the IB10B core (see fig. S2 and Supplementary Text). Slightly above the stratigraphic range of these species in the IB10B core [from 80 to 77 m below surface (mbs)], we record a ~4‰ negative CIE in total organic carbon (TOC) and in palynological residue (Fig. 1). The presence of *Morozovella acuta* [last occurrence, 54.7 Ma (*31*)] above the CIE in the IB10B core implies that this CIE represents the PETM (see Supplementary Text for detailed stratigraphy).

The general $\delta^{13}C_{TOC}$ pattern is mimicked in the $\delta^{13}C$ measured on the isolated palynological residues ($\delta^{13}C_{paly}$), which mainly consists of dinoflagellate cysts (dinocysts). However, $\delta^{13}C_{paly}$ values are up to ~7‰ higher than $\delta^{13}C_{TOC}$ values in the interval between 80 and 77 mbs (Fig. 1B). This interval has relatively high TOC and dinocyst concentrations 2- to 50-fold higher than below (Fig. 1D), pointing to high marine productivity. This likely caused high $\delta^{13}C_{DIC}$ values that, in turn, lead to high $\delta^{13}C_{paly}$ and $\delta^{13}C_{TOC}$, in fact close to the Paleocene value for $\delta^{13}C_{TOC}$. We therefore place the onset of the CIE at ~80 mbs. The onset of the CIE is followed by an interval with stable $\delta^{13}C$ values up to ~70 mbs, often referred to as the "body" of the CIE, and a subsequent gradual recovery phase to ~65 mbs, suggesting that the PETM in our record is complete [see the study by Bowen (*32*) and references therein].

For the SQ, a 2‰ negative CIE in foraminifer carbonate at the top of the section slightly above the P4c/P5 planktonic foraminifer zone boundary suggests the presence of the onset of the PETM (*19*). However, not all foraminifer isotope records are consistent with this inference. In addition, overlying strata are affected by weathering, and planktonic foraminifer abundances decrease (*19*). Therefore, only pre-PETM temperatures can be inferred unambiguously from the SQ, and we focus on the IB10B core for the PETM.

[1]Marine Palynology and Paleoceanography, Laboratory of Palaeobotany and Palynology, Department of Earth Sciences, Faculty of Geosciences, Utrecht University, Heidelberglaan 2, 3584CS Utrecht, Netherlands. [2]Geologische Bundesanstalt, Neulinggasse 38, A 1030 Wien, Austria. [3]Department of Earth, Atmospheric, and Planetary Sciences, Purdue University, West Lafayette, IN 47906, USA. [4]Department of Geology and Mineral Sciences, University of Ilorin, P.M.B. 1515, Kwara State, Nigeria. [5]Department of Earth Sciences, Faculty of Geosciences, Utrecht University, Heidelberglaan 2, 3584CS Utrecht, Netherlands. [6]NIOZ Royal Netherlands Institute for Sea Research, Department of Marine Microbiology and Biogeochemistry, and Utrecht University, 't Horntje, Texel, Netherlands.
*Corresponding author. Email: j.frieling1@uu.nl

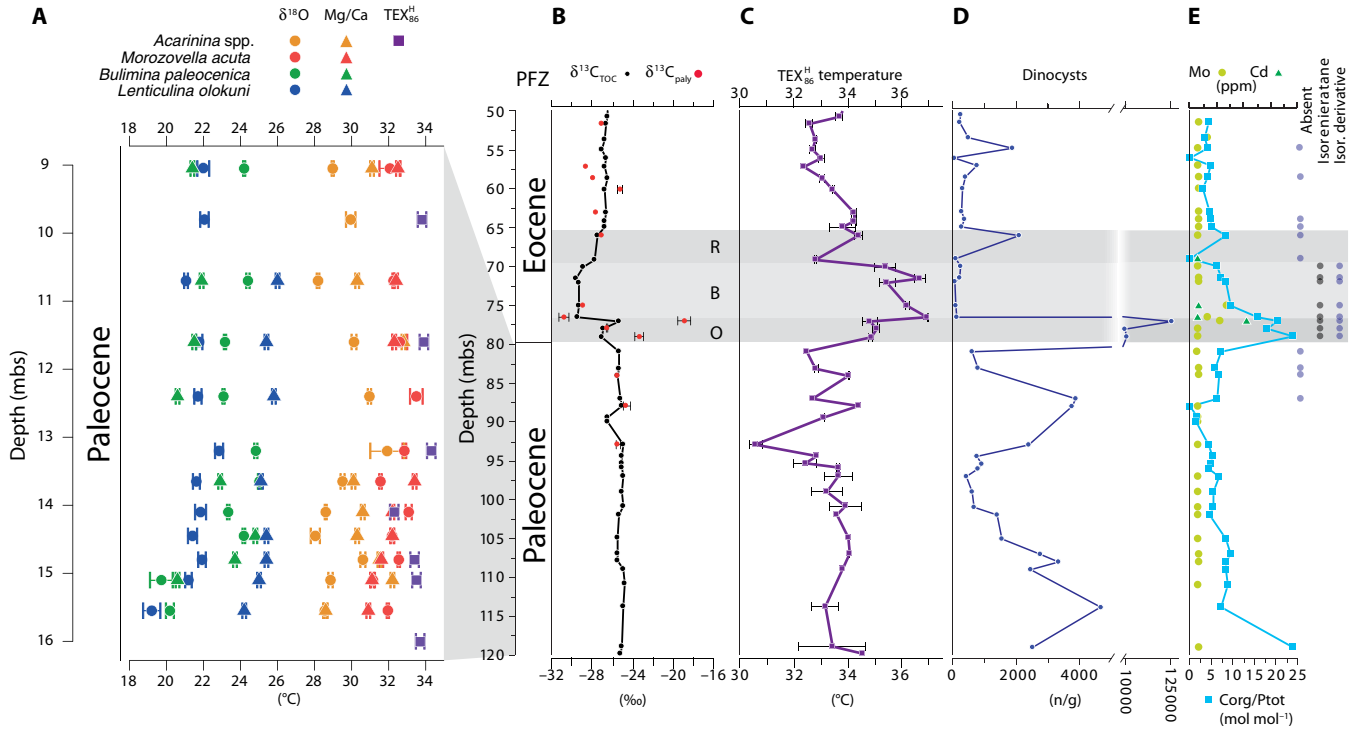

Fig. 1. Temperature and environment for the SQ (A) and IB10B core (B to E). (**A**) SQ surface and bottom-water temperature reconstructions based on Mg/Ca (triangles), $\delta^{18}O$ (circles) of selected foraminifer species, and TEX_{86}^{H} (squares). Error bars represent analytical errors. Conservative 1σ calibration errors: 1.6°C for $\delta^{18}O$; 1.7° and 2°C for planktonic and benthic Mg/Ca, respectively; and 2.5°C for TEX_{86}^{H}. (**B**) IB10B stable carbon isotope record of TOC ($\delta^{13}C_{TOC}$) and palynological residue ($\delta^{13}C_{paly}$). The phases of the CIE are denoted by O, B, and R for onset, body, and recovery, respectively. PFZ, planktonic foraminifer zone. (**C**) TEX_{86}^{H}-based SST (error bars based on replicate measurements). (**D**) Absolute concentrations of dinocysts per gram of dry sediment. Note the scale break between 4,000 and 10,000. (**E**) Indicators of anoxia: Organic carbon over total phosphorus ratio (Corg/Ptot) (blue squares). Presence of isorenieratene and its derivative. Concentrations of redox-sensitive trace elements Mo (light green circles) and Cd (dark green triangles) in parts per million (ppm). Note that Mo concentrations are close to the detection limit, and absolute values should be treated with caution.

For sea surface temperature (SST) reconstructions, we use the TEX_{86}^{H} paleothermometer (*33*), based on the relative abundances of membrane lipids of marine Thaumarchaeota (see Supplementary Text for calibration and potential caveats). TEX_{86}^{H} indicates average latest Paleocene SSTs of 33.6 ± 0.4°C (n = 7) and 33.4 ± 0.2°C (n = 9) based on the sediments from the SQ and the IB10B core, respectively (Fig. 1, A and C). The reconstructed SSTs exceed the range of the modern ocean core-top calibration by ~4°C, and thus, care has to be taken in interpreting these values. However, in mesocosm experiments (*34*), archaeal membrane lipids have shown a continuous linear relation with temperature up to 40°C, which provides support for extrapolation. If a linear TEX_{86} calibration, such as the Bayesian calibration (*35*), or any of the mesocosm calibrations (*33*) were used, then reconstructed SSTs would be higher (see Supplementary Text for detailed discussion).

We also reconstruct Paleocene SSTs by analyzing the Mg/Ca ratios and the oxygen isotopic composition ($\delta^{18}O$) of glassy, mixed-layer–dwelling planktonic foraminifers *Acarinina* spp. (mostly *Acarinina nitida* and *Acarinina soldadoensis*) and *M. acuta* from the SQ only, because foraminifera from the IB10 cores are unfortunately poorly preserved. For Mg/Ca, we assume Paleocene seawater Mg/Ca of 2 mol mol^{-1}, correct for the nonlinear response under changing Mg/Ca (*36*), and use calibrations for planktonic (*37*) and benthic (*38*) foraminifera to calculate seawater temperatures. We assume a local seawater $\delta^{18}O$ of −0.39‰, correcting for the latitude (+0.61‰) and the absence of large ice sheets (−1.0‰) (see Supplementary Text) to calculate seawater temperatures (*39*). Mg/Ca and $\delta^{18}O$ temperatures derived from *Acarinina* average 31.0 ± 0.6°C and 29.5 ± 0.5°C, respectively, whereas *M. acuta* yields 32.2 ± 0.4°C and 31.4 ± 0.3°C, respectively. *M. acuta* likely had a shallower depth habitat than *Acarinina* spp., based on their respective $\delta^{13}C$ and $\delta^{18}O$ values (*3*), consistent with our data. Therefore, Mg/Ca and $\delta^{18}O$ of *M. acuta* and TEX_{86}^{H} provide consistent latest Paleocene SST estimates, well within the proxy calibration error, of 32° to 34°C (Fig. 1, A and C). Mg/Ca and $\delta^{18}O$ of the benthic foraminifera *Bulimina paleocenica* and *Lenticulina olokuni* indicate seafloor (100 to 150 m) temperatures of ~23°C (Fig. 1A).

We compare these reconstructions with output from new simulations carried out with the National Center for Atmospheric Research (NCAR) Community Earth System Model (CESM1) using well-established Eocene boundary conditions (*30*). Late Paleocene and Early Eocene temperatures are better constrained than CO_2 concentrations based on proxy data. We therefore compare temperatures from proxies and CESM1 model runs and find that they favorably match in the simulations, with radiative forcings equivalent to 2240 and 4480 ppm of CO_2, similar to work with the previous model version (*28*). We therefore refer to these simulations as the "latest Paleocene" and "PETM" cases, although these CO_2 concentrations exceed Early Eocene proxy estimates (*40*). The latest Paleocene simulation (34.3°C) reproduces the Nigerian latest Paleocene SSTs reconstructed here (32° to 34°C) and supports the strong temperature stratification at the core location as inferred from the data (Figs. 1A and 2, A and B). The model results

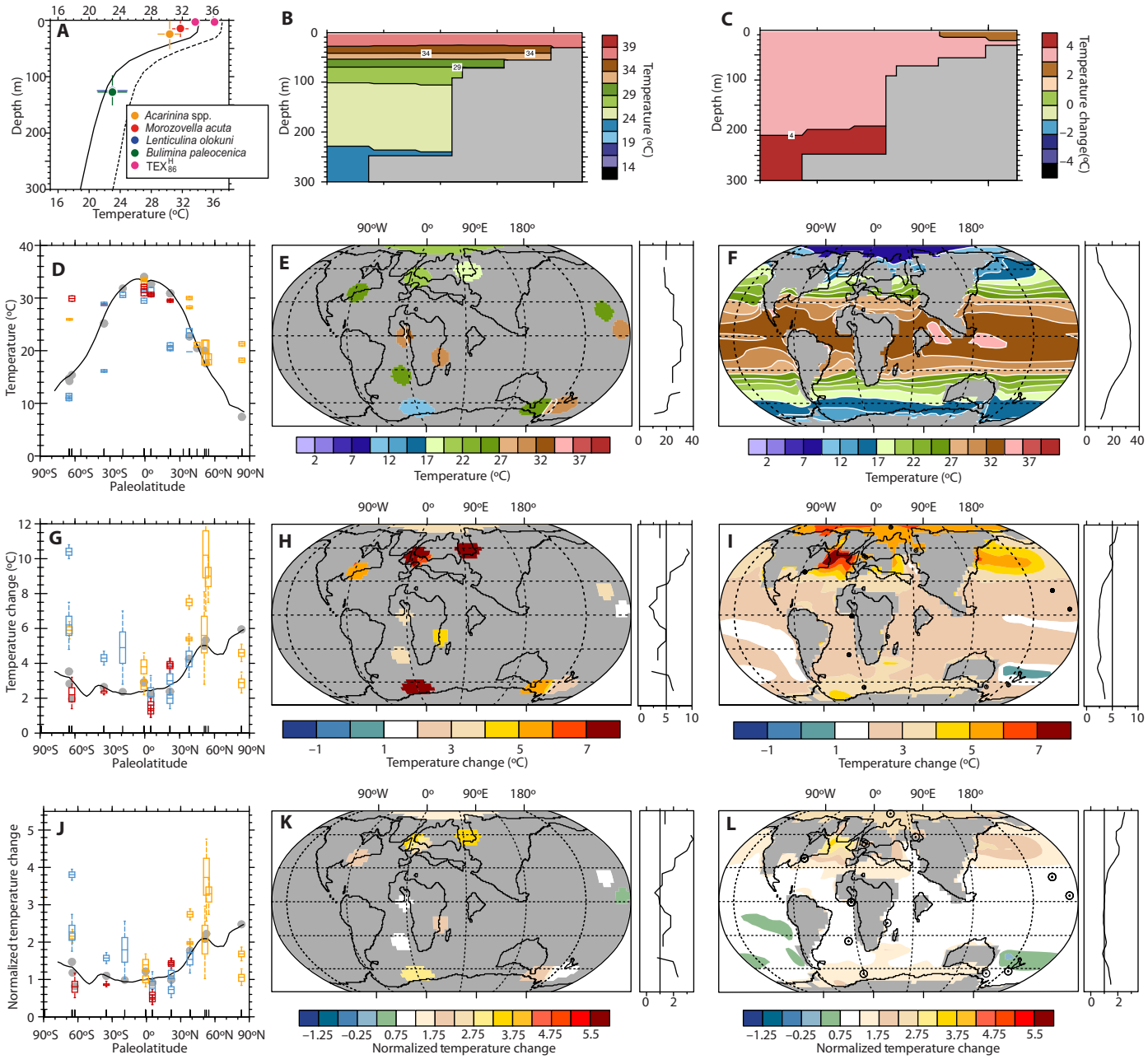

Fig. 2. Model-data comparison for latest Paleocene (2240 ppm) and PETM (4480 ppm) CO_2 scenarios. (**A**) Vertical temperature profile for the site locations. Solid and dashed lines represent latest Paleocene and PETM model estimates, respectively. Data from Fig. 1 (A and C) for comparison, including error bars for depth: *Morozovella* (0 to 30 m), *Acarinina* (0 to 50 m), TEX_{86}^H (0 m; surface), and benthic (100 to 150 m). (**B**) Modeled latest Paleocene temperature along an inshore-offshore transect representing the study site. (**C**) Modeled warming from latest Paleocene to PETM along the same transect. (**D**) TEX_{86}^H-derived (orange), $\delta^{18}O$-derived (blue), and Mg/Ca-derived (red) SSTs and modeled Paleocene meridional SST gradient (solid line). Gray dots represent point-by-point model-data comparisons. (**E**) Interpolated absolute SST reconstructions. (**F**) Modeled latest Paleocene (2240 ppm) temperatures. (**G**) PETM absolute SST changes and TEX_{86}^H-derived (orange), $\delta^{18}O$-derived (blue), and Mg/Ca-derived (red) SST changes between the latest Paleocene and the PETM. Gray dots represent point-by-point model-data comparisons. (**H**) Interpolated change in absolute SST. (**I**) Modeled SST change from the latest Paleocene to the PETM (2240 to 4480 ppm). (**J**) PETM SST changes, normalized to tropical (20°N to 20°S) SST changes (2.7°C) from the data and TEX_{86}^H-derived (orange), $\delta^{18}O$-derived (blue), and Mg/Ca-derived (red) SST changes between the latest Paleocene and the PETM. Gray dots represent point-by-point model-data comparisons. (**K**) SST changes from the latest Paleocene to the PETM from the data, normalized to tropical SST changes in the data (2.7°C). (**L**) SST changes from the latest Paleocene to the PETM, normalized to tropical SST changes in CESM1 (2.4°C). Black circles indicate site locations.

further suggest that this basin represented some of the warmest open ocean temperatures in the Early Paleogene world (Fig. 2H), making this a suitable location to record the effects of extreme greenhouse warming on biota during the PETM.

SSTs during the body of the PETM CIE averaged 36.1 ± 0.7°C (n = 5) based on TEX_{86}^H from the IB10B core, implying average warming of ~3°C relative to the latest Paleocene (Fig. 1C). Other TEX_{86} calibrations typically imply a greater degree of warming and higher maximum

temperatures (see the Supplementary Materials), indicating that the TEX_{86}^{H} calibration–based SST change may represent a conservative estimate. No mixed-layer planktonic foraminifera and only few poorly preserved thermocline-dwelling foraminifera were found in the PETM section of the IB10B core, hampering Mg/Ca and $\delta^{18}O$ paleothermometry. The temperatures are within the range of plausible planktonic foraminifer $\delta^{18}O$-derived SSTs from the western tropical Indian Ocean (*12*) and model results (Fig. 2, D and E). The maximum recorded absolute SST of 37°C, about 8°C warmer than any open ocean at present, is reached at ~76.5 mbs. These results are consistent with the simulations, in terms of both relative change and absolute values (Fig. 2A).

Recent modeling work has succeeded in reproducing most proxy reconstructions, with the exception of the Arctic Ocean and the southwest Pacific Ocean (*28*). The simulations presented here have the same shortcomings. Crucially, however, our SST data for the background latest Paleocene–earliest Eocene climate state support the very warm tropical oceans of >35°C that are necessary to approach these warm extratropics in models. In addition, the hot tropical SSTs refute tropical thermostat theory (*14*).

Our data, together with the few other tropical records [Ocean Drilling Project (ODP) site 865 and Tanzania] from a global compilation of proxy records (see Supplementary Text), imply that the mean warming of the tropical oceans was ~3°C. Mid- and high-latitude regions warmed by 5° to 8°C (*2*, *3*, *5*), implying that ocean warming was amplified somewhat in the extratropics during the PETM, contrary to previous reconstructions (*2*, *10*). Other TEX_{86} calibrations produce the same qualitative result, although with a somewhat smaller magnitude of extratropical amplification.

In the modern ocean, spatial temperature gradients are weak in the tropics compared to mid and high latitudes, and they were likely even weaker during the latest Paleocene and PETM because of smaller latitudinal and surface–deep ocean gradients. This means that the few available records likely represent trends and values in the entire tropical band reasonably well. To identify whether the model and data show the same pattern of extratropical amplification and to be able to compare between models, we therefore normalize regional temperature changes by the averaged observed tropical (20°N to 20°S) temperature change. This approach highlights that most extratropical regions warm only slightly more than the tropics in both data and model (Fig. 2, J to L) throughout the Atlantic Ocean and in the central Pacific Ocean. The largest disagreements are from 50°N to 60°N and 50°S to 60°S latitude, where the proxies show much greater amplification than the models. The only truly polar proxy record, from the Arctic, shows no clear signal of polar amplification, as noted previously (*2*), in sharp contrast to the model.

More data, in particular from multiproxy records, are necessary to make a definitive statement about the ability of the current generation of climate models to reproduce past meridional temperature gradient responses to PETM warming. However, we believe that the normalizing approach has merit because the resulting pattern is a specific "fingerprint" that may be used as a test of models.

Based on optimal interpolation on the proxy records and by taking area-weighted means, we find that global tropical mean SSTs increased by 2.7°C across the PETM and that the global mean SSTs increased by 5.3°C, very close to previous estimates (*4*), but our estimate avoids the use of an intervening climate model. CESM1 has a modern equilibrium climate sensitivity of 3.2°C per doubling of CO_2, and we find a similar response of 3.5°C for a doubling under Eocene conditions in our simulations. However, the global mean SST change is only 2.8°C per doubling, indicating that the 3.5°C global response reflects enhanced warming on land. Thus, a model with this sensitivity would require nearly two further doublings of CO_2 (or equivalent forcing) to achieve a global mean SST increase of 5.3°C, as implied by the data. The required carbon release would then be >10,000 giga–metric tons (Gt) of carbon, which is in keeping with budgets from other climate models (*41*). These large carbon inputs and resulting CO_2 values are unlikely (*42*) and not supported by recent pCO_2 (partial pressure of CO_2) estimates (*43*). Hence, the most likely explanation is that the latest Paleocene equilibrium climate sensitivity was significantly larger than the model's 3.2°C, perhaps due to strongly increased sensitivity at higher temperature (*44*) during the PETM, or non-CO_2 changes in radiative balance were of importance in maintaining latest Paleocene warmth and enhancing PETM warming (*45*).

Finally, to investigate the impact of the extremely high SSTs on biota, we investigated dinocyst assemblages. Upper Paleocene dinocyst assemblages in the IB10 core and SQ represent normal marine assemblages, similar to those in extratropical regions during the PETM (*5*, *46*). However, at many of these sites, the peak of the PETM is characterized by high productivity of marine dinocysts (*46*, *47*). Our data from Nigeria show the opposite. At ~77 mbs, we record a decrease from 10^5 to less than 10^2 dinocysts per gram of dry sediment (Fig. 1D). The remaining dinocyst assemblages are impoverished with only heterotrophic and generalist genera (see Supplementary Text). Intermittent anoxia developed at the study site during the PETM, evidenced by the presence of the biomarker isorenieratene and a diagenetic derivative, and enrichment of redox-sensitive trace elements (see Fig. 1E and Supplementary Text). Dinocyst assemblages suggest enhanced stratification during periods of strongest anoxia at the onset of the CIE, based on trace elements and the absence of benthic foraminifer linings (fig. S3). Crucially, however, these extreme conditions apparently did not negatively affect dinocyst diversity or concentrations; in fact dinocyst concentrations peak in this interval (Fig. 1D). We therefore consider it unlikely that apparently less extreme anoxia and stratification during the body of the CIE caused the demise of dinoflagellates. We also do not find evidence for a preservation bias or indications of enhanced runoff in dinocyst assemblages or pollen and spore concentrations (see fig. S3 and Supplementary Text).

Instead, we surmise that conditions became too hot for most dinoflagellate taxa during the body of the PETM, when SSTs rose to values >36°C. Such temperatures are considered uninhabitable for most marine eukaryotic organisms today (*48*) even for hardy dinoflagellates, which are among the most temperature-resilient eukaryote plankton groups (*49*). Apart from often displaying narrow temperature tolerance ranges (*9*), many modern thermophilic organisms show a sharp decline in productivity and, consequently, survival above optimum temperatures (*50*). A similar absence of mixed-layer planktonic foraminifera was observed in Tanzania (*12*), suggesting that heat stress may have been more widespread in tropical marginal marine settings during the PETM.

No similar temporal absence of eukaryotic plankton has been observed in tropical regions during the extreme warmth of OAE2 (Oceanic Anoxic Event 2), across the Cenomanian-Turonian transition (~94 Ma), where comparable TEX_{86}^{H} temperature estimates were obtained (*51*). This suggests that the rate of change during the PETM was an important factor in creating a heat-induced eukaryotic marine plankton dead zone at this tropical location. Given that the rates of modern carbon input and warming are estimated to exceed those of the

PETM by ~10 times (*52*), our results suggest that tropical oceans will be subject to warming and significant biotic change over the coming centuries at rates that may exceed those of the PETM.

MATERIALS AND METHODS

Materials

Paleocene and Eocene sediments in the Dahomey Basin are classified in three major formations: Paleocene limestones of the Ewekoro Formation, Paleocene-Eocene uniform gray to dark gray shales of the Oshosun Formation, and Eocene Ilaro sandstones (*18*). These formations can be traced laterally over the Dahomey Basin (fig. S1). For this study, we analyzed samples from the Oshosun Formation, in the Nigerian sector of the Dahomey Basin (fig. S1) from the SQ and the two drill cores IB10A and IB10B. The Oshosun Formation ranges in thickness from ~18 m in the SQ (*19*) to ~110 m in the IB10 cores (*20*). Concretionary horizons, as observed in the SQ by Gebhardt *et al.* (*19*), were not observed in the IB10 cores.

Samples from the Oshosun and Ewekoro formations from the SQ (6°48′12.54″N and 3°37′46.11″E) were collected during a field expedition in 2003 and used for foraminifer and dinoflagellate analyses for biostratigraphy (*19*, *20*). From the 13 samples from the Oshosun Formation, we used ~5 to 10 g for quantitative dinocyst analysis, ~10 g for biomarker geochemistry, and 0.3 g for stable bulk organic carbon isotope ($\delta^{13}C_{TOC}$) measurements. Approximately 600 g was disintegrated, sieved, and picked as aliquots or completely for foraminifera (*19*). Pristine (glassy and hollow) specimens of *M. acuta*, *Acarinina* spp., *B. paleocenica*, and *L. olokuni*, which are common to abundant throughout the section, were selected for stable isotope and trace element analyses.

The sediments from two drill cores, IB10A and IB10B (6°53′N and 3°00′E), were recovered during the exploration drilling in 1976, targeting the Paleocene limestones of the Ewekoro Formation, near Ilaro, Nigeria. In 2001, samples from IB10A and IB10B were taken for foraminifer biostratigraphy. Samples from IB10A from a published study (*20*) were used for a pilot. In 2012, we took 73 samples from the 110-m-long IB10B core. Each sample was split into several fractions: 2 to 10 g for palynological analysis, 5 to 10 g for organic geochemistry, 1 g for major and trace element analyses, and 0.3 g for $\delta^{13}C_{TOC}$. The remaining core material is stored at the Nigerian Geological Survey Core Repository in Abuja, Nigeria. Residues of washed samples, scanning electron microscopy (SEM) stubs, and slides with picked foraminifera from the SQ are stored in the collection of the Geological Survey of Austria, Vienna, Austria (collection nos. GBA2010/122/0001 to GBA2010/122/0053). Palynological slides, residues, and organic extracts are stored at the Laboratory of Palaeobotany and Palynology, Utrecht University (Utrecht, Netherlands).

Methods

Micropaleontology.

Foraminifera. Air-dried sediment (600 g) was disintegrated with 5% hydrogen peroxide and washed over a 63-μm sieve. Residues were air-dried, split into aliquots, and completely picked for foraminifera with a dry paintbrush. Samples with insufficient amounts of sample material were discarded. For stable isotope and Mg/Ca analyses of the SQ foraminifera, we exclusively used pristine (that is, glassy and hollow) specimens (see SEM images for wall profiles, fig. S2). Foraminifera from the IB10B and IB10A cores were only used for biostratigraphy because of their frosty appearance, indicating postsedimentary recrystallization.

Palynology. We processed and analyzed a total of 53 samples from IB10B, 19 samples from IB10A, and 7 samples from the SQ using standard protocols at the Laboratory of Palaeobotany and Palynology, Utrecht University (*5*). A spike (n = 18583 ± 762) of exotic spores, *Lycopodium clavatum*, was added to 5 to 10 g of the freeze-dried sample to allow for absolute quantitative analysis. HCl (10%) was added to dissolve carbonates. Supernatants were subsequently decanted, and residues were treated twice with 38 to 40% HF and 30% HCl to remove silicates. After decantation, residues were washed with tap water over 250- and 15-μm sieves to remove large and small particles, respectively. One drop of the concentrated residue was mounted on a microscope slide using glycerin jelly, and a minimum of 200 dinocysts were counted, if possible. For several samples across the body of the PETM, up to four microscope slides were counted to a total of 18 to 134 dinocysts. Assemblages for these samples are thus statistically less well constrained than those for the samples with ≥200 counted dinocysts. However, because *Lycopodium* spores were also abundant in these slides, this does not affect quantification of absolute numbers of dinocysts per gram of sediment.

Organic matter stable carbon isotope analyses.

For stable isotope analysis of bulk organic carbon ($\delta^{13}C_{TOC}$), 0.3 g of freeze-dried material was powdered and decalcified using 1 M HCl. Samples were dried in a stove at 50°C, and subsequently, TOC content was measured on ~10 mg of powdered, homogenized residue using a CNS analyzer (Fisons). Stable carbon isotope ratios were determined using an isotope ratio mass spectrometer (IRMS; Finnigan DELTAplus) coupled online to the CNS analyzer. Absolute reproducibility, based on international and in-house standards, for TOC and $\delta^{13}C_{TOC}$ was better than 0.1% and 0.05‰, respectively.

For stable carbon isotope measurements of the palynological residue ($\delta^{13}C_{paly}$), an aliquot was washed over a 40-μm sieve with distilled water to remove the *Lycopodium* spores and most other pollen and spores to obtain a fraction that mostly contains dinocysts, along with some other palynomorphs. Because of the small amounts of large pollen and spores and low amounts of phytoclasts, the fraction typically consists of dinocysts (~90+%) and foraminifer linings (maximum, 10%). The body of the CIE is dominated by organic material from foraminifer linings and minor contributions from dinoflagellates. Of this residue, 15 to 30 μg was weighed and analyzed on the same IRMS. Samples of sufficient weight were measured in duplicate.

Foraminifer geochemistry.

Stable isotope analyses. We picked multiple specimens from each SQ sample. These aliquots comprise about 10 specimens of *L. olokuni*, about 100 specimens of *B. paleocenica*, about 20 specimens of *Acarinina* spp., and about 10 specimens of *M. acuta*. Note that we used mixed *Acarinina* species because of their relatively low abundance. *A. nitida* was the most abundant species within *Acarinina*.

Foraminiferal tests were treated with 98.8% ethanol, cracked, and ultrasonically cleaned. Stable carbon and oxygen isotopes were measured on a Finnigan MAT 251 mass spectrometer at Leibniz-Labor (Kiel), coupled online to the Carbo-Kiel device I for automated CO_2 preparation. External precision is better than 0.20‰ (average, 0.04‰) and 0.19‰ (average, 0.04‰) for oxygen and carbon, respectively. Data are given in conventional delta notation versus Vienna Pee Dee Belemnite standard.

Mg/Ca ratios. We picked multiple foraminifera from each SQ sample to measure Mg/Ca ratios. These aliquots comprise about 10 specimens of *L. olokuni* (0.23 to 1.53 mg), about 100 specimens of *B. paleocenica* (0.10 to 0.71 mg), about 20 specimens of *Acarinina* spp. (0.18 to 0.80 mg), and about 10 specimens of *M. acuta* (0.24 to 0.89 mg). As for stable isotope analyses, we used mixed *Acarinina* species because of their

relatively low abundance. The cleaning protocol included several steps for removing adhering clays and siliciclastic particles, and a reduction step (anhydrous hydrazine) for removing ferromanganese coatings (*21*). Foraminiferal tests were analyzed on an inductively coupled plasma atomic emission spectroscopy instrument with an Mg/Ca intensity ratio calibration according to de Villiers *et al.* (*22*) at Leibniz-Labor (Kiel). Internal analytical precision is better than 0.1 to 0.2% relative standard deviation.

Biomarker analyses.

For TEX_{86} analysis (51 samples), ~10 g of freeze-dried, powdered sediment was extracted by a Dionex accelerated solvent extractor using dichloromethane DCM:Methanol (9:1, v/v) at 100°C and 7×10^6 Pa. Extracts were separated into polar and apolar fractions over an Al_2O_3 column using methanol/DCM (1:1) and hexane/DCM (9:1) as respective eluents. Apolar fractions of 18 samples across the PETM CIE were measured by gas chromatography using an Agilent 6890 gas chromatograph and by gas chromatography–mass spectrometry using a Thermo DSQ mass spectrometer to identify isorenieratene and its diagenetic derivatives.

To analyze glycerol dibiphytanyl glycerol tetraethers (GDGTs), hexane:isopropanol (99:1) was added to the polar fraction, filtered over a 0.45-µm polytetrafluoroethylene filter, and subsequently measured for GDGTs on an Agilent 1290 ultrahigh-performance liquid chromatography mass spectrometer at Utrecht University. We measured in-house standards to monitor consistency in TEX_{86} and branched isoprenoid tetraether (BIT) values. Most samples were measured in duplicate, some in triplicate, to assess reproducibility. Reproducibility was always better than 0.02 TEX_{86} units and 0.1 BIT units, and reproducibility of in-house standards was always better than 0.01 and 0.03 for TEX_{86} and BIT, respectively.

We used the BIT index (*23*) and methane indices (MIs) (*24*, *25*) to assess influences of terrestrial, methanotrophic, and methanogenic GDGT producers on TEX_{86}. BIT values below 0.3 (*26*) or 0.4 (*27*) generally yield trustworthy TEX_{86} values. A weak correlation exists between TEX_{86} and BIT ($r^2 = 0.168$; fig. S4), but samples with BIT values of >0.3 are not statistically different from those with BIT values of <0.3. We therefore used all TEX_{86} data, except for one outlier (that is, more than 2 SDs from the mean), at 93 mbs. GDGT-2/GDGT-3 ratios are close to normal shallow marine ratios (two to three) rather than reflecting GDGT distributions influenced by diffusive methane fluxes (about nine) (*24*). Likewise, the cutoff (0.3) for the MI of Zhang *et al.* (*25*) was never reached.

Bulk sediment chemistry.

Approximately 125 mg of freeze-dried sediment was dissolved in 2.5 ml of HF (40%) and 2.5 ml of $HClO_4/HNO_3$ mixture in a closed Teflon bomb at 90°C during one night. The acids were then evaporated at 160°C, and the resulting gel was subsequently redissolved in 1 M HNO_3 at 90°C during another night. Subsequently, total elemental concentrations were determined by inductively coupled plasma optical emission spectrometry (PerkinElmer Optima 3000). Precision and accuracy were better than 5%, based on calibration to standard solutions and checked against internal laboratory standard sediments.

Climate modeling.

We carried out a suite of simulations using the NCAR CESM1, using our well-established boundary conditions. This includes a T31 spectral resolution atmosphere and ~1.8° × 3° horizontal spacing and 25 vertical levels for the oceans. Simulations spanned a range of radiative forcings equivalent to 1120, 2240, and 4480 ppm of CO_2. All these simulations were carried out for >3000 years and were fully equilibrated as indicated by ocean temperature trends, surface and top-of-atmosphere energy imbalance, and trends in ideal age tracers. The higher CO_2-forced experiments produce climates that compare favorably with temperature proxy records for the latest Paleocene and Early Eocene, which is similar to the results we found with the previous version of the NCAR model (*6*, *28*); we will refer to these as the latest Paleocene and PETM simulations. As described previously, the low CO_2 simulations match Late Eocene climates well (*29*). We also conducted short sensitivity studies, using new high-resolution earliest Eocene boundary conditions (*30*) within a model with higher resolution (atmosphere, 2° × 2° horizontal finite volume resolution; ocean, 1° × 1° and 40 vertical levels). Although these simulations were not fully equilibrated in the deep ocean, they established that the upper ocean temperature gradients found in the lower-resolution simulations were robust.

All sites within 20° of the equator were averaged to define the tropical mean. In this case, this includes the following sites: Tanzania, Nigeria, and ODP site 865 (table S2). The findings are qualitatively insensitive to the choice of what to normalize by.

We used standard techniques in ocean data assimilation to create homogenized and interpolated maps of SSTs based on the sparse data. The proxy records treated according to the standard oceanographic technique of Barnes-Cressman iterated objective analysis implemented in the NCAR Command Language (www.ncl.ucar.edu/Document/Functions/Contributed/obj_anal_ic_Wrap.shtml). In this approach, each observation is assigned a circular radius of influence, *R*. Here, we used successive values of *R* of 10°, 2°, and 1°. A first guess of the value at every grid point was made by including all observations within the region of influence of that grid point. A distance-weighted average of the differences between the first-guess fields and the actual observations was made, and this anomaly was added into the first-guess fields to calculate a second-guess field. Thus, observations from beyond the radius of influence were ignored in updating the field, and other observations closer to the initial observation were given greater weight. This was done for all grid points under consideration. The resulting fields were used as the basis for the next iteration, which was carried out with a smaller region of influence.

SUPPLEMENTARY MATERIALS

Supplementary material for this article is available at http://advances.sciencemag.org/cgi/content/full/3/3/e1600891/DC1

Supplementary Text

fig. S1. Geological map of the Nigerian sector of the Dahomey Basin.

fig. S2. Wall profiles for analyzed foraminifer species from the SQ.

fig. S3. Environmental reconstructions for the IB10B core.

fig. S4. IB10A and IB10B TEX_{86} and BIT correlations.

fig. S5. Bayesian TEX_{86} calibrations using the IB10B data set and BAYSPAR tool (https://figshare.com/articles/BAYSPAR_Matlab_Prediction_Code/1352033) (*46*, *69*).

fig. S6. IB10B chemostratigraphy and stratigraphical ranges of selected foraminifera and dinocysts.

fig. S7. IB10A chemostratigraphy and stratigraphical ranges of selected foraminifera and dinocysts.

fig. S8. Sensitivity plots for $\delta^{18}O_w$ and Mg/Ca_{sw}.

table S1. Dinocyst assemblages for the Sagamu Quarry.

table S2. Sea surface temperature (SST) data used in Figure 2D, E, G, H.

References (*53*–*100*)

REFERENCES AND NOTES

1. G. R. Dickens, M. M. Castillo, J. C. G. Walker, A blast of gas in the latest Paleocene: Simulating first-order effects of massive dissociation on oceanic methane hydrate. *Geology* **25**, 259–262 (1997).
2. A. Sluijs, S. Schouten, M. Pagani, M. Woltering, H. Brinkhuis, J. S. Sinninghe Damsté, G. R. Dickens, M. Huber, G.-J. Reichart, R. Stein, J. Matthiessen, L. J. Lourens, N. Pedentchouk, J. Backman, K. Moran, Expedition 302 Scientists, Subtropical Arctic

Ocean temperatures during the Palaeocene/Eocene Thermal Maximum. *Nature* **441**, 610–613 (2006).
3. J. C. Zachos, S. Schouten, S. Bohaty, T. Quattlebaum, A. Sluijs, H. Brinkhuis, S. J. Gibbs, T. J. Bralower, Extreme warming of mid-latitude coastal ocean during the Paleocene-Eocene Thermal Maximum Inferences from TEX_{86} and isotope data. *Geology* **34**, 737–740 (2006).
4. T. Dunkley Jones, D. J. Lunt, D. N. Schmidt, A. Ridgwell, A. Sluijs, P. J. Valdes, M. Maslin, Climate model and proxy data constraints on ocean warming across the Paleocene–Eocene Thermal Maximum. *Earth Sci. Rev.* **125**, 123–145 (2013).
5. A. Sluijs, P. K. Bijl, S. Schouten, U. Röhl, G.-J. Reichart, H. Brinkhuis, Southern ocean warming, sea level and hydrological change during the Paleocene-Eocene Thermal Maximum. *Clim. Past* **7**, 47–61 (2011).
6. D. J. Lunt, T. Dunkley Jones, M. Heinemann, M. Huber, A. LeGrande, A. Winguth, C. Loptson, J. Marotzke, C. D. Roberts, J. Tindall, P. Valdes, C. Winguth, A model–data comparison for a multi-model ensemble of early Eocene atmosphere–ocean simulations: EoMIP. *Clim. Past* **8**, 1717–1736 (2012).
7. M. Huber, A hotter greenhouse? *Science* **321**, 353–354 (2008).
8. S. C. Sherwood, M. Huber, An adaptability limit to climate change due to heat stress. *Proc. Natl. Acad. Sci. U.S.A.* **107**, 9552–9555 (2010).
9. J. M. Sunday, A. E. Bates, N. K. Dulvy, Global analysis of thermal tolerance and latitude in ectotherms. *Proc. Biol. Sci.* **278**, 1823–1830 (2011).
10. J. C. Zachos, M. W. Wara, S. Bohaty, M. L. Delaney, M. R. Petrizzo, A. Brill, T. J. Bralower, I. Premoli-Silva, A transient rise in tropical sea surface temperature during the Paleocene-Eocene Thermal Maximum. *Science* **302**, 1551–1554 (2003).
11. R. Kozdon, D. C. Kelly, N. T. Kita, J. H. Fournelle, J. W. Valley, Planktonic foraminiferal oxygen isotope analysis by ion microprobe technique suggests warm tropical sea surface temperatures during the Early Paleogene. *Paleoceanography* **26**, PA3206 (2011).
12. T. Aze, P. N. Pearson, A. J. Dickson, M. P. S. Badger, P. R. Bown, R. D. Pancost, S. J. Gibbs, B. T. Huber, M. J. Leng, A. L. Coe, A. S. Cohen, G. L. Foster, Extreme warming of tropical waters during the Paleocene–Eocene Thermal Maximum. *Geology* **42**, 739–742 (2014).
13. S. Solomon, G.-K. Plattner, R. Knutti, P. Friedlingstein, Irreversible climate change due to carbon dioxide emissions. *Proc. Natl. Acad. Sci. U.S.A.* **106**, 1704–1709 (2009).
14. I. N. Williams, R. T. Pierrehumbert, M. Huber, Global warming, convective threshold and false thermostats. *Geophys. Res. Lett.* **36**, L21805 (2009).
15. M. Setona, R. D. Müllera, S. Zahirovica, C. Gainab, T. Torsvikb, G. Shepharda, A. Talsmaa, M. Gurnisf, M. Turnerf, S. Maush, M. Chandlerg, Global continental and ocean basin reconstructions since 200 Ma. *Earth Sci. Rev.* **113**, 212–270 (2012).
16. D. J. J. van Hinsbergen, L. V. de Groot, S. J. van Schaik, W. Spakman, P. K. Bijl, A. Sluijs, C. G. Langereis, H. Brinkhuis, A paleolatitude calculator for paleoclimate studies. *PLOS ONE* **10**, e0126946 (2015).
17. E. A. Okosun, A review of the Cretaceous stratigraphy of the Dahomey Embayment, West Africa. *Cretac. Res.* **11**, 17–27 (1990).
18. H. G. Billman, Offshore stratigraphy and paleontology of the Dahomey Embayment, 7th Africa Micropaleontology Paleontology, Ile-Ife, Ile-Ife, Nigeria, 1976, pp. 21–46.
19. H. Gebhardt, O. A. Adekeye, S. O. Akande, Late Paleocene to Initial Eocene Thermal Maximum (IETM) foraminiferal biostratigraphy and paleoecology of the Dahomey Basin, Southwestern Nigeria. *Jahrb. Geol. Bundesanst.* **3**, 407–419 (2011).
20. S. I. Bankole, E. Schrank, B.-D. Erdtmann, Palynology of the Paleogene Oshosun Formation in the Dahomey Basin, southwestern Nigeria. *Rev. Esp. Micropaleontol.* **39**, 29–44 (2007).
21. P. Martin, A simple evaluation of cleaning procedures on fossil benthic foraminiferal Mg/Ca. *Geochem. Geophys. Geosyst.* **3**, 1–8 (2002).
22. S. de Villiers, M. Greaves, H. Elderfield, An intensity ratio calibration method for the accurate determination of Mg/Ca and Sr/Ca of marine carbonates by ICP-AES. *Geochem. Geophys. Geosyst.* **3**, 2001GC000169 (2002).
23. E. C. Hopmans, J. W. H. Weijers, E. Schefuß, L. Herfort, J. S. Sinninghe Damsté, S. Schouten, A novel proxy for terrestrial organic matter in sediments based on branched and isoprenoid tetraether lipids. *Earth Planet. Sci. Lett.* **224**, 107–116 (2004).
24. J. W. H. Weijers, K. L. H. Lim, A. Aquilina, J. S. Sinninghe Damsté, R. D. Pancost, Biogeochemical controls on glycerol dialkyl glycerol tetraether lipid distributions in sediments characterized by diffusive methane flux. *Geochem. Geophys. Geosyst.* **12**, Q10010 (2011).
25. C. L. Zhanga, X.-L. Liud, L. Lic, K.-U. Hinrichsd, J. E. Noakese, Methane index: A tetraether archaeal lipid biomarker indicator for detecting the instability of marine gas hydrates. *Earth Planet. Sci. Lett.* **307**, 525–534 (2011).
26. J. W. H. Weijers, S. Schouten, O. C. Spaargaren, J. S. Sinninghe Damsté, Occurrence and distribution of tetraether membrane lipids in soils: Implications for the use of the TEX_{86} proxy and the BIT index. *Org. Geochem.* **37**, 1680–1693 (2006).
27. P. K. Bijl, J. A. P. Bendle, S. M. Bohaty, J. Pross, S. Schouten, L. Tauxe, C. E. Stickley, R. M. McKay, U. Röhl, M. Olney, A. Sluijs, C. Escutia, H. Brinkhuis; Expedition 318 Scientists, Eocene cooling linked to early flow across the Tasmanian Gateway. *Proc. Natl. Acad. Sci. U.S.A.* **110**, 9645–9650 (2013).
28. M. Huber, R. Caballero, The early Eocene equable climate problem revisited. *Clim. Past* **7**, 603–633 (2011).
29. A. Goldner, N. Herold, M. Huber, Antarctic glaciation caused ocean circulation changes at the Eocene–Oligocene transition. *Nature* **511**, 574–577 (2014).
30. N. Herold, J. Buzan, M. Seton, A. Goldner, J. A. M. Green, R. D. Müller, P. Markwick, M. Huber, A suite of early Eocene (~55 Ma) climate model boundary conditions. *Geosci. Model Dev.* **7**, 2077–2090 (2014).
31. B. S. Wade, P. N. Pearson, W. A. Berggren, H. Pälike, Review and revision of Cenozoic tropical planktonic foraminiferal biostratigraphy and calibration to the geomagnetic polarity and astronomical time scale. *Earth Sci. Rev.* **104**, 111–142 (2011).
32. G. J. Bowen, Up in smoke: A role for organic carbon feedbacks in Paleogene hyperthermals. *Glob. Planet. Change* **109**, 18–29 (2013).
33. J.-H. Kim, J. van der Meer, S. Schouten, P. Helmke, V. Willmott, F. Sangiorgi, N. Koç, E. C. Hopmans, J. S. Sinninghe Damsté, New indices and calibrations derived from the distribution of crenarchaeal isoprenoid tetraether lipids: Implications for past sea surface temperature reconstructions. *Geochim. Cosmochim. Acta* **74**, 4639–4654 (2010).
34. S. Schouten, A. Forster, F. E. Panoto, J. S. Sinninghe Damsté, Towards calibration of the TEX_{86} palaeothermometer for tropical sea surface temperatures in ancient greenhouse worlds. *Org. Geochem.* **38**, 1537–1546 (2007).
35. J. E. Tierney, M. P. Tingley, A Bayesian, spatially-varying calibration model for the TEX_{86} proxy. *Geochim. Cosmochim. Acta* **127**, 83–106 (2014).
36. D. Evans, W. Müller, Deep time foraminifera Mg/Ca paleothermometry: Nonlinear correction for secular change in seawater Mg/Ca. *Paleoceanography* **27**, PA4205 (2012).
37. P. Anand, H. Elderfield, M. H. Conte, Calibration of Mg/Ca thermometry in planktonic foraminifera from a sediment trap time series. *Paleoceanography* **18**, 1050 (2003).
38. C. H. Lear, Y. Rosenthal, N. Slowey, Benthic foraminiferal Mg/Ca-paleothermometry: A revised core-top calibration. *Geochim. Cosmochim. Acta* **66**, 3375–3387 (2002).
39. S.-T. Kim, J. R. O'Neil, Equilibrium and nonequilibrium oxygen isotope effects in synthetic carbonates. *Geochim. Cosmochim. Acta* **61**, 3461–3475 (1997).
40. E. Anagnostou, E. H. John, K. M. Edgar, G. L. Foster, A. Ridgwell, G. N. Inglis, R. D. Pancost, D. J. Lunt, P. N. Pearson, Changing atmospheric CO_2 concentration was the primary driver of early Cenozoic climate. *Nature* **533**, 380–384 (2016).
41. K. J. Meissner, T. J. Bralower, K. Alexander, T. Dunkley Jones, W. Sijp, M. Ward, The Paleocene-Eocene Thermal Maximum: How much carbon is enough? *Paleoceanography* **29**, 946–963 (2014).
42. K. Panchuk, A. Ridgwell, L. R. Kump, Sedimentary response to Paleocene-Eocene Thermal Maximum carbon release: A model-data comparison. *Geology* **36**, 315–318 (2008).
43. A. Gehler, P. D. Gingerich, A. Pack, Temperature and atmospheric CO_2 concentration estimates through the PETM using triple oxygen isotope analysis of mammalian bioapatite. *Proc. Natl. Acad. Sci. U.S.A.* **113**, 7739–7744 (2016).
44. J. Bloch-Johnson, R. T. Pierrehumbert, D. S. Abbot, Feedback temperature dependence determines the risk of high warming. *Geophys. Res. Lett.* **42**, 4973–4980 (2015).
45. J. T. Kiehl, C. A. Shields, Sensitivity of the Palaeocene–Eocene Thermal Maximum climate to cloud properties. *Philos. Trans. R. Soc. A* **371**, 20130093 (2013).
46. A. Sluijs, H. Brinkhuis, A dynamic climate and ecosystem state during the Paleocene-Eocene Thermal Maximum: Inferences from dinoflagellate cyst assemblages at the New Jersey Shelf. *Biogeosciences* **6**, 1755–1781 (2009).
47. I. C. Harding, A. J. Charles, J. E. A. Marshall, H. Pälike, A. P. Roberts, P. A. Wilson, E. Jarvis, R. Thorne, E. Morris, R. Moremon, R. B. Pearce, S. Akbari, Sea-level and salinity fluctuations during the Paleocene–Eocene Thermal Maximum in Arctic Spitsbergen. *Earth Planet. Sci. Lett.* **303**, 97–107 (2011).
48. G. N. Somero, Proteins and temperature. *Annu. Rev. Physiol.* **57**, 43–68 (1995).
49. G. M. Hallegraeff, J. P. Valentine, J.-A. Marshall, C. J. Bolch, Temperature tolerances of toxic dinoflagellate cysts: Application to the treatment of ships' ballast water. *Aquat. Ecol.* **31**, 47–52 (1997).
50. H. W. Paerl, N. S. Hall, E. S. Calandrino, Controlling harmful cyanobacterial blooms in a world experiencing anthropogenic and climatic-induced change. *Sci. Total Environ.* **409**, 1739–1745 (2011).
51. A. Forster, S. Schouten, K. Moriya, P. A. Wilson, J. S. Sinninghe Damsté, Tropical warming and intermittent cooling during the Cenomanian/Turonian oceanic anoxic event 2: Sea surface temperature records from the equatorial Atlantic. *Paleoceanography* **22**, PA1219 (2007).
52. R. E. Zeebe, A. Ridgwell, J. C. Zachos, Anthropogenic carbon release rate unprecedented during the past 66 million years. *Nat. Geosci.* **9**, 325–329 (2016).
53. M.-P. Aubry, K. Ouda, C. Dupuis, W. A. Berggren, J. A. Van Couvering, The Global Standard Stratotype-Section and Point (GSSP) for the base of the Eocene Series in the Dababiya section (Egypt). *Episodes* **30**, 271–286 (2007).
54. E. M. Crouch, C. Heilmann-Clausen, H. Brinkhuis, H. E. G. Morgans, K. M. Rogers, H. Egger, B. Schmitz, Global dinoflagellate event associated with the late Paleocene Thermal Maximum. *Geology* **29**, 315–318 (2001).

55. E. M. Crouch, G. R. Dickens, H. Brinkhuis, M.-P. Aubry, C. J. Hollis, K. M. Rogers, H. Visscher, The *Apectodinium* acme and terrestrial discharge during the Paleocene–Eocene Thermal Maximum New palynological, geochemical and calcareous nannoplankton observations at Tawanui, New Zealand. *Palaeogeogr. Palaeoclimatol. Palaeoecol.* **194**, 387–403 (2003).
56. J. P. Bujak, H. Brinkhuis, Global warming and dinocyst changes across the Paleocene/Eocene epoch boundary, in *Late Paleocene-Early Eocene Climatic and Biotic Events in the Marine and Terrestrial Records*, M.-P. Aubry, S. Lucas, W. A. Berggren, Eds. (Columbia Univ. Press, 1998), pp. 277–295.
57. A. Sluijs, H. Brinkhuis, S. Schouten, S. M. Bohaty, C. M. John, J. C. Zachos, G.-J. Reichart, J. S. Sinninghe Damsté, E. M. Crouch, G. R. Dickens, Environmental precursors to rapid light carbon injection at the Palaeocene/Eocene boundary. *Nature* **450**, 1218–1221 (2007).
58. E. Guasti, T. J. Kouwenhoven, H. Brinkhuis, R. P. Speijer, Paleocene sea-level and productivity changes at the southern Tethyan margin (El Kef, Tunisia). *Mar. Micropaleontol.* **55**, 1–17 (2005).
59. E. M. Crouch, H. Brinkhuis, H. Visscher, T. Adatte, M.-P. Bolle, Late Paleocene-early Eocene dinoflagellate cyst records from the Tethys: Further observations on the global distribution of Apectodinium. *Spec. Pap. Geol. Soc. Am.* **369**, 113–131 (2003).
60. A. I. Iakovleva, H. Brinkhuis, C. Cavagnetto, Late Palaeocene–Early Eocene dinoflagellate cysts from the Turgay Strait, Kazakhstan; correlations across ancient seaways. *Palaeogeogr. Palaeoclimatol. Palaeoecol.* **172**, 243–268 (2001).
61. L. J. Lourens, A. Sluijs, D. Kroon, J. C. Zachos, E. Thomas, U. Röhl, J. Bowles, I. Raffi, Astronomical pacing of late Palaeocene to early Eocene global warming events. *Nature* **435**, 1083–1087 (2005).
62. Y. Cui, L. R. Kump, A. J. Ridgwell, A. J. Charles, C. K. Junium, A. F. Diefendorf, K. H. Freeman, N. M. Urban, I. C. Harding, Slow release of fossil carbon during the Palaeocene-Eocene Thermal Maximum. *Nat. Geosci.* **4**, 481–485 (2011).
63. S. Bains, R. M. Corfield, R. D. Norris, Mechanisms of climate warming at the end of the paleocene. *Science* **285**, 724–727 (1999).
64. C. M. John, S. M. Bohaty, J. C. Zachos, A. Sluijs, S. Gibbs, H. Brinkhuis, T. J. Bralower, North American continental margin records of the Paleocene-Eocene Thermal Maximum Implications for global carbon and hydrological cycling. *Paleoceanography* **23**, PA2217 (2008).
65. F. A. McInerney, S. L. Wing, The Paleocene-Eocene Thermal Maximum A perturbation of carbon cycle, climate, and biosphere with implications for the future. *Annu. Rev. Earth Planet. Sci.* **39**, 489–516 (2011).
66. R. M. Coggon, D. A. H. Teagle, C. E. Smith-Duque, J. C. Alt, M. J. Cooper, Reconstructing past seawater Mg/Ca and Sr/Ca from mid-ocean ridge flank calcium carbonate veins. *Science* **327**, 1114–1117 (2010).
67. J. B. Creech, J. A. Baker, C. J. Hollis, H. E. G. Morgans, E. G. C. Smith, Eocene sea temperatures for the mid-latitude southwest Pacific from Mg/Ca ratios in planktonic and benthic foraminifera. *Earth Planet. Sci. Lett.* **299**, 483–495 (2010).
68. J. C. Zachos, L. D. Stott, K. C. Lohmann, Evolution of early Cenozoic marine temperatures. *Paleoceanography* **9**, 353–387 (1994).
69. T. H. Torsvik, R. Van der Voo, U. Preeden, C. Mac Niocaill, B. Steinberger, P. V. Doubrovine, D. J. J. van Hinsbergen, M. Domeier, C. Gaina, E. Tohver, J. G. Meert, P. J. A. McCausland, L. R. M. Cocks, Phanerozoic polar wander, palaeogeography and dynamics. *Earth Sci. Rev.* **114**, 325–368 (2012).
70. J. Bijma, W. W. Faber, C. Hemleben, Temperature and salinity limits for growth and survival of some planktonic foraminifers in laboratory cultures. *J. Foraminiferal Res.* **20**, 95–116 (1990).
71. M. S. Lachniet, Climatic and environmental controls on speleothem oxygen-isotope values. *Quat. Sci. Rev.* **28**, 412–432 (2009).
72. R. E. Zeebe, Seawater pH and isotopic paleotemperatures of Cretaceous oceans. *Palaeogeogr. Palaeoclimatol. Palaeoecol.* **170**, 49–57 (2001).
73. J. Uchikawa, R. E. Zeebe, Examining possible effects of seawater pH decline on foraminiferal stable isotopes during the Paleocene-Eocene Thermal Maximum. *Paleoceanography* **25**, PA2216 (2010).
74. D. E. Penman, B. Hönisch, R. E. Zeebe, E. Thomas, J. C. Zachos, Rapid and sustained surface ocean acidification during the Paleocene-Eocene Thermal Maximum. *Paleoceanography* **29**, 357–369 (2014).
75. C. Huguet, G. J. de Lange, Ö. Gustafsson, J. J. Middelburg, J. S. Sinninghe Damsté, S. Schouten, Selective preservation of soil organic matter in oxidized marine sediments (Madeira Abyssal Plain). *Geochim. Cosmochim. Acta* **72**, 6061–6068 (2008).
76. G. N. Inglis, A. Farnsworth, D. Lunt, G. L. Foster, C. J. Hollis, M. Pagani, P. E. Jardine, P. N. Pearson, P. Markwick, A. M. J. Galsworthy, L. Raynham, K. W. R. Taylor, R. D. Pancost, Descent towards the Icehouse: Eocene sea surface cooling inferred from GDGT distributions. *Paleoceanography* **30**, 1000–1020 (2015).
77. G. Trommer, M. Siccha, M. T. J. van der Meer, S. Schouten, J. S. Sinninghe Damsté, H. Schulz, C. Hemleben, M. Kucera, Distribution of Crenarchaeota tetraether membrane lipids in surface sediments from the Red Sea. *Org. Geochem.* **40**, 724–731 (2009).
78. A. Pearson, A. E. Ingalls, Assessing the use of archaeal lipids as marine environmental proxies. *Annu. Rev. Earth Planet. Sci.* **41**, 359–384 (2013).
79. S. Schouten, E. C. Hopmans, A. Rosell-Melé, A. Pearson, P. Adam, T. Bauersachs, E. Bard, S. M. Bernasconi, T. S. Bianchi, J. J. Brocks, L. Truxal Carlson, I. S. Castañeda, S. Derenne, A. Doğrul Selver, K. Dutta, T. Eglinton, C. Fosse, V. Galy, K. Grice, K.-U. Hinrichs, Y. Huang, A. Huguet, C. Huguet, S. Hurley, A. Ingalls, G. Jia, B. Keely, C. Knappy, M. Kondo, S. Krishnan, S. Lincoln, J. Lipp, K. Mangelsdorf, A. Martínez-García, G. Ménot, A. Mets, G. Mollenhauer, N. Ohkouchi, J. Ossebaar, M. Pagani, R. D. Pancost, E. J. Pearson, F. Peterse, G.-J. Reichart, P. Schaeffer, G. Schmitt, L. Schwark, S. R. Shah, R. W. Smith, R. H. Smittenberg, R. E. Summons, Y. Takano, H. M. Talbot, K. W. R. Taylor, R. Tarozo, M. Uchida, B. E. van Dongen, B. A. S. Van Mooy, J. Wang, C. Warren, J. W. H. Weijers, J. P. Werne, M. Woltering, S. Xie, M. Yamamoto, H. Yang, C. L. Zhang, Y. Zhang, M. Zhao, J. S. Sinninghe Damsté, An interlaboratory study of TEX_{86} and BIT analysis of sediments, extracts, and standard mixtures. *Geochem. Geophys. Geosyst.* **14**, 5263–5285 (2013).
80. J. E. Tierney, in *Reconstructing Earth's Deep-Time Climate—The State of the Art in 2012*, L. C. Ivany, B. T. Huber, Eds. (The Paleontological Society Papers, 2012), vol. 18, pp. 115–131.
81. C. Wuchter, S. Schouten, S. G. Wakeham, J. S. Sinninghe Damsté, Archaeal tetraether membrane lipid fluxes in the northeastern Pacific and the Arabian Sea: Implications for TEX_{86} paleothermometry. *Paleoceanography* **21**, PA4208 (2006).
82. M. T. Hernández-Sánchez, E. M. S. Woodward, K. W. R. Taylor, G. M. Henderson, R. D. Pancost, Variations in GDGT distributions through the water column in the South East Atlantic Ocean. *Geochim. Cosmochim. Acta* **132**, 337–348 (2014).
83. J.-H. Kim, S. Schouten, M. Rodrigo-Gámiz, S. Rampen, G. Marino, C. Huguet, P. Helmke, R. Buscail, E. C. Hopmans, J. Pross, F. Sangiorgi, J. B. M. Middelburg, J. S. Sinninghe Damsté, Influence of deep-water derived isoprenoid tetraether lipids on the paleothermometer in the Mediterranean Sea. *Geochim. Cosmochim. Acta* **150**, 125–141 (2015).
84. S. L. Ho, T. Laepple, Flat meridional temperature gradient in the early Eocene in the subsurface rather than surface ocean. *Nat. Geosci.* **9**, 606–610 (2016).
85. A. Sluijs, S. Schouten, T. H. Donders, P. L. Schoon, U. Röhl, G.-J. Reichart, F. Sangiorgi, J.-H. Kim, J. S. Sinninghe Damsté, H. Brinkhuis, Warm and wet conditions in the Arctic region during Eocene Thermal Maximum 2. *Nat. Geosci.* **2**, 777–780 (2009).
86. J. H. Kim, S. Schouten, E. C. Hopmans, B. Donner, J. S. Sinninghe Damsté, Global sediment core-top calibration of the TEX86 paleothermometer in the ocean. *Geochim. Cosmochim. Acta* **72**, 1154–1173 (2008).
87. J. Frieling, A. I. Iakovleva, G.-J. Reichart, G. N. Aleksandrova, Z. N. Gnibidenko, S. Schouten, A. Sluijs, Paleocene–Eocene warming and biotic response in the epicontinental West Siberian Sea. *Geology* **42**, 767–770 (2014).
88. P. L. Schoon, C. Heilmann-Clausen, B. P. Schultz, J. S. Sinninghe Damsté, S. Schouten, Warming and environmental changes in the eastern North Sea Basin during the Palaeocene–Eocene Thermal Maximum as revealed by biomarker lipids. *Org. Geochem.* **78**, 79–88 (2015).
89. C. J. Hollis, B. R. Hines, K. Littler, V. Villasante-Marcos, D. K. Kulhanek, C. P. Strong, J. C. Zachos, S. M. Eggins, L. Northcote, A. Phillips, The Paleocene–Eocene Thermal Maximum at DSDP Site 277, Campbell Plateau, southern Pacific Ocean. *Clim. Past* **11**, 1009–1025 (2015).
90. K. A. F. Zonneveld, G. J. M. Versteegh, M. Kodrans-Nsiah, Preservation and organic chemistry of Late Cenozoic organic-walled dinoflagellate cysts: A review. *Mar. Micropaleontol.* **68**, 179–197 (2008).
91. J. S. Sinninghe Damsté, J. Koster, M. Baas, M. P. Koopmans, H. M. E. van Kaam-Peters, J. A. J. Geenevasen, C. Kruk, Cyclisation and aromatisation of carotenoids during sediment diagenesis. *J. Chem. Soc. Chem. Commun.*, 187–188 (1995).
92. A. Sluijs, U. Röhl, S. Schouten, H.-J. Brumsack, F. Sangiorgi, J. S. Sinninghe Damsté, H. Brinkhuis, Article late Paleocene–early Eocene paleoenvironments with special emphasis on the Paleocene-Eocene Thermal Maximum (Lomonosov Ridge, Integrated Ocean Drilling Program Expedition 302). *Paleoceanography* **23**, PA1S11 (2008).
93. A. Sluijs, L. van Roij, G. J. Harrington, S. Schouten, J. A. Sessa, L. J. LeVay, G.-J. Reichart, C. P. Slomp, Warming, euxinia and sea level rise during the Paleocene–Eocene Thermal Maximum on the gulf coastal plain: Implications for ocean oxygenation and nutrient cycling. *Clim. Past* **10**, 1421–1439 (2014).
94. T. W. Lyons, A. D. Anbar, S. Severmann, C. Scott, B. C. Gill, Tracking euxinia in the ancient ocean: A multiproxy perspective and proterozoic case study. *Annu. Rev. Earth Planet. Sci.* **37**, 507–534 (2009).
95. E. D. Ingall, R. M. Bustin, P. Van Cappellen, Influence of water column anoxia on the burial and preservation of carbon and phosphorus in marine shales. *Geochim. Cosmochim. Acta* **57**, 303–316 (1993).
96. R. A. Fensome, J. B. Riding, F. J. R. Taylor, in *Palynology: Principles and Application*, J. Jansonius, D. C. McGregor, Eds. (American Association of Stratigraphic Palynologists Foundation, 1996), pp. 107–169.
97. M. T. Madigan, J. M. Martinko, P. V. Dunlap, D. P. Clark, Brock biology of microorganisms 12th edn. *Int. Microbiol.* **11**, 65–73 (2008).
98. V. J. Paul, in *Cyanobacterial Harmful Algal Blooms: State of the Science and Research Needs* (Springer, 2008), pp. 239–257.

99. A. Sluijs, J. Pross, H. Brinkhuis, From greenhouse to icehouse; organic-walled dinoflagellate cysts as paleoenvironmental indicators in the Paleogene. *Earth Sci. Rev.* **68**, 281–315 (2005).
100. J. Barke, J. van der Burgh, J. H. A. van Konijnenburg-van Cittert, M. E. Collinson, M. A. Pearce, J. Bujak, C. Heilmann-Clausen, E. N. Speelman, M. M. L. van Kempen, G.-J. Reichart, A. F. Lotter, H. Brinkhuis, Coeval Eocene blooms of the freshwater fern *Azolla* in and around Arctic and Nordic seas. *Palaeogeogr. Palaeoclimatol. Palaeoecol.* **337–338**, 108–119 (2012).

Acknowledgments: We thank N. Welters, A. van Dijk, M. Egger, J. Weijers (Utrecht University), J. Ossebaar, and A. Mets (Royal Netherlands Institute for Sea Research) and G. Bartoli (Kiel) for analytical advice and support and E. Schrank (Technical University of Berlin) for pointing us to the study sections. **Funding:** The European Research Council (ERC) under the European Union Seventh Framework Program provided funding for this work (ERC starting grant 259627 to A.S.). The Netherlands Organization for Scientific Research supported this work through grant 834.11.006 to G.-J.R. Fieldwork of H.G. in AQ55 Nigeria was funded by Volkswagen Foundation (AZ: I/77 620). The German Academic Exchange Service and the Nigerian Petroleum Technology Development Fund provided funding to S.O.A. and O.A.A. M.H. acknowledges funding through NSF OCE 0902882 and EPS 1101245, and computing was provided by the Rosen Center for Advanced Computing at Purdue. This work was carried out under the program of the Netherlands Earth System Science Centre, financially supported by the Ministry of Education, Culture and Science. **Author contributions:** J.F., A.S., H.G., G.-J.R., and S.O.A. designed the study. O.A.A., S.O.A., and H.G. analyzed carbonate microfossil stratigraphy and chemistry. J.F., G.-J.R., and S.S. performed organic geochemical analyses. J.F. and A.S. performed palynological analyses. J.J.M., J.F., G.-J.R., and A.S. analyzed inorganic geochemical data. M.H. performed NCAR Climate System Model studies. J.F., A.S., and M.H. wrote the paper, with input from all authors. All authors analyzed and discussed the data. **Competing interests:** J.J.M. is a governing board member of Netherlands Institute of Sea Research and advisory board member of MPI-Marine Microbiology, Bremen; GEOMAR, Kiel; MARUM, Bremen; Red Sea Center, KAUST, SA. The other authors declare that they have no competing interests. **Data and materials availability:** All data needed to evaluate the conclusions in the paper are present in the paper and/or the Supplementary Materials. Additional data related to this paper may be requested from the authors. All data used in this paper can be found in the online database Pangaea.

Submitted 25 April 2016
Accepted 27 December 2016
Published 3 March 2017
10.1126/sciadv.1600891

Citation: J. Frieling, H. Gebhardt, M. Huber, O. A. Adekeye, S. O. Akande, G.-J. Reichart, J. J. Middelburg, S. Schouten, A. Sluijs, Extreme warmth and heat-stressed plankton in the tropics during the Paleocene-Eocene Thermal Maximum. *Sci. Adv.* **3**, e1600891 (2017).

Extreme warmth and heat-stressed plankton in the tropics during the Paleocene-Eocene Thermal Maximum

Joost Frieling, Holger Gebhardt, Matthew Huber, Olabisi A. Adekeye, Samuel O. Akande, Gert-Jan Reichart, Jack J. Middelburg, Stefan Schouten and Appy Sluijs

Sci Adv **3** (3), e1600891.
DOI: 10.1126/sciadv.1600891